Biosensors and Bioelectronics 25 (2010) 1640–1645

Contents lists available at ScienceDirect

Biosensors and Bioelectronics

journal homepage: www.elsevier.com/locate/bios

Electrochemical DNA biosensor fabrication with hollow gold nanospheres modified electrode and its enhancement in DNA immobilization and hybridization

Shufeng Liu*, Jing Liu, Xiaoping Han, Yanning Cui, Wei Wang

Key Laboratory of Eco-chemical Engineering, Ministry of Education, College of Chemistry and Molecular Engineering, Qingdao University of Science and Technology, Qingdao 266042, China

ARTICLE INFO

Article history:
Received 5 September 2009
Received in revised form
26 November 2009
Accepted 27 November 2009
Available online 2 December 2009

Keywords:
DNA immobilization
DNA hybridization
Hollow gold nanospheres
Electrochemical biosensor

ABSTRACT

In this article, hollow gold nanospheres (HGN) were prepared by using Co nanoparticles as sacrificial templates and varying the stoichiometric ratio of $HAuCl_4$ over the reductants. The HGN was then modified on the electrode surface via a 1,6-hexanedithiol linking agent to fabricate a novel electrochemical DNA biosensor. The whole DNA biosensor fabrication process was characterized by cyclic voltammetry (CV) and electrochemical impedance spectroscopy (EIS) methods with the use of ferricyanide as an electrochemical redox indicator. The probe DNA immobilization and hybridization on the modified electrode was further studied with CV and differential pulse voltammetry (DPV) methods by using $Co(phen)_3^{3+}$ as an electrochemical hybridization indicator. Results revealed that the HGN modified electrode, especially for the HGN with the outer surface surrounded by densely spike-like nanocrystallites, could largely enhance the DNA hybridization ability. The fabricated DNA biosensor was proved to have a low detection limit (1 pM) and a wide dynamic range (from 1 pM to 10 nM) with a high stability and reusability.

1. Introduction

The development of DNA biosensors has recently attracted substantial attentions in connection with research efforts directed at gene analysis, the detection of genetic disorders, tissue matching, and forensic applications (Taton et al., 2000; Gunnarsson et al., 2008). Many techniques including fluorescence (Yang et al., 2008; Duan et al., 2007), electrochemiluminescence (Zhu et al., 2008; Zhang et al., 2008a,b), electrochemistry (Kara et al., 2002; Drummond et al., 2003), surface plasmon resonance spectroscopy (Kim et al., 2007) and quartz crystal microbalance (Patolsky et al., 2000; Minunni et al., 2005) have been developed for the DNA detection. Among them electrochemical techniques offer a lot of advantages such as simplicity, rapidness, low-cost and high sensitivity (Zhang et al., 2009a,b; March et al., 2008). Many protocols have been proposed for electrochemical monitoring of DNA hybridization (Munde et al., 2007; Gorodetsky et al., 2008).

A key issue with any DNA hybridization biosensor is how to enhance the probe DNA immobilization amount, and moreover maintain the accessibility of probe DNA for hybridization detection (Kjällman et al., 2008; Liu et al., 2005; Cederquist et al., 2008). In order to enhance the immobilization amount of probe DNA and optimize the DNA hybridization efficiency, different kinds of strategies have been developed (Liu et al., 2008; Gasparac et al., 2004). Including which, nanomaterials have been paid a great deal of attention in electrode surface modification for DNA biosensor fabrication owing to their increased surface area, improved electrochemical properties and possible beneficial orientation effect in DNA immobilization and hybridization. These nanomaterials used for electrode surface modification includes metal nanoparticles (Li et al., 2007; Liu et al., 2005), semiconductor nanoparticles (Du et al., 2009), nanowires (Zhang et al., 2008a,b), carbon nanotube (Basuray et al., 2009; Zhang et al., 2009a,b), nanopores (Hu et al., 2008), etc. Among all the nanomaterials, gold nanoparticles are the most frequently used for electrode surface modification in the fabrication of biosensor (Yamada et al., 2003; Zhao et al., 2007; Jena and Raj, 2007; Cai et al., 2001; Liu et al., 2002a,b).

Recently, hollow metallic particles have received a lot of attentions because of their use as drug carriers, electrocatalytic materials, etc. owing to the distinctive advantages of low density, high specific surface area, and reduction of costs compared with their solid counterparts (Sun and Xia, 2002a, 2002b; Liang et al., 2004; Guo et al., 2007). Various templates, including polystyrene spheres, silica spheres, vesicles, microemulsion and metal nanoparticles, etc., have been used to fabricate hollow spheres (Kim et al., 2002; Schmidt and Ostafin, 2002; Wong et al., 2002; Sun and Xia, 2002a,b; Lu et al., 2005; Lu et al., 2007). Whereas the application of hollow metal spheres in biosensor fabrication was still very less

* Corresponding author. Tel.: +86 532 84022681; fax: +86 532 84022681.
E-mail address: shufengliu77@yahoo.com (S. Liu).

0956-5663/$ – see front matter © 2009 Elsevier B.V. All rights reserved.
doi:10.1016/j.bios.2009.11.026

reported to date. In the field of DNA biosensor fabrication, Lu et al. (2005, 2007) have originally prepared a hollow gold ball with the use of vesicle as a template and further studied its ability in enhancing DNA immobilization and hybridization. Usually, these prepared hollow spheres are in the micro or pseudo micro-meter scale and also not readily operated in the preparation and electrode surface modification. Therefore, it is of great importance to develop the simple preparation method of hollow gold nanospheres (HGN) and explore this kind of special nanomaterials for the application in DNA biosensor fabrication.

In this research, the HGN were simply fabricated based on the displacement reaction between the Co nanoparticles and $HAuCl_4$. The prepared HGN showed a rough hollow ball structure surrounded with dense spike-like gold nanocrystallites. It is specially profit for DNA immobilization and hybridization. The current research focuses on the DNA immobilization and hybridization events on the HGN modified electrode and provides a suitable platform for the DNA biosensor fabrication.

2. Experimental

2.1. Chemicals and materials

Cobalt (II) chloride hexahydrate ($CoCl_2{\cdot}6H_2O$, 99.0%), tetrachloroaurate(III) tetrahydrate ($HAuCl_4{\cdot}4H_2O$, 47.8% Au) were obtained from National Chemical Reagent Ltd., Shanghai, China. Sodium borohydride ($NaBH_4$, 99%) was purchased from Acros Organics (USA). 1,6-hexanedithiol was purchased from Sigma (USA). The tris(1,10-phenanthroline) Cobalt (III) perchlorate, $Co(phen)_3(ClO_4)_3$, was synthesized as that reported in the literature (Gillard et al., 1983). $K_3Fe(CN)_6$, $K_4Fe(CN)_6$ were purchased from Tianjin Ruijinte Chemical Co. Ltd. (China). All other chemicals were all of analytical grade and used without further purification. Doubly distilled water was used throughout.

All of synthetic oligonucleotides were purchased from SBS Genetech. Co. Ltd. (China). Their base sequences are listed as follows:

Probe DNA: 5′-SH-GCG CGA ACC GTA TA-3′
Complementary target DNA: 5′-TAT ACG GTT CGC GC-3′
Non-complementary target DNA: 5′-ACT GAT GCT ACC AT-3′

2.2. Apparatus

Cyclic voltammetry (CV) and differential pulse voltammetry (DPV) measurements were performed with a CHI832B electrochemical analyzer (Shanghai CH Instrument Company, China). Electrochemical impedance spectroscopy (EIS) measurements were carried out on a CHI660C electrochemical workstation (Shanghai CH Instrument Company, China). All electrochemical experiments were performed with a conventional three-electrode system comprising a gold working electrode, a platinum wire auxiliary electrode, and a Ag/AgCl reference electrode. The EIS measurements were performed in 1.0 mM $K_3[Fe(CN)_6]$ containing 0.10 M KCl with the frequency range from 10^4 to 0.01 Hz.

2.3. Fabrication of hollow gold nanospheres (HGN)

The HGN were prepared according to the reference (Liang et al., 2005) with a slight modification. For the synthesis of HGN, the Co nanoparticles were first prepared. The synthesis of Co nanoparticles was carried out based on the reported method (Kobayashi et al., 2003). The Co nanoparticles could be easily obtained with the addition of 0.2 mL of 0.4 M $CoCl_2$ solution into 200 mL of deaerated aqueous solution containing 8 mM $NaBH_4$ and 0.8 mM citric acid. The nitrogen gas was bubbled before mixing for 20 min and continued during the reaction in order to avoid the oxidation of obtained Co nanoparticles by existed atmospheric oxygen in the solution. The hydrogen gas was observed to be evolved during the reaction and continued for several minutes. Following with the end of gas evolution, 30 mL of Co nanoparticle colloidal solutions were extracted and transferred to different volumes (5, 8, 12, 18 and 40 mL, respectively) of stirred 1 mM $HAuCl_4$ aqueous solutions to achieve the preparation of the HGN. The obtained suspension solutions were centrifuged at 10,000 rps and the precipitates were designated as samples A–E.

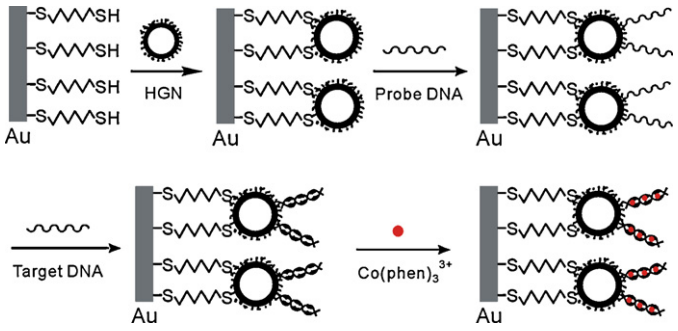

Fig. 1. Schematic illustration of the fabrication steps of the electrochemical DNA biosensor.

2.4. DNA biosensor fabrication

The gold working electrode surface was freshly polished prior to use with 0.05 μm alumina powder and then cleaned ultrasonically sequentially in acetone and water for 3 min. The whole DNA biosensor fabrication process was schematically demonstrated in Fig. 1. The detailed procedures for DNA biosensor fabrication are listed in the AppendixBSupplementary Information.

2.5. DNA hybridization detection with an electrochemical indicator of $Co(phen)_3^{3+}$

The probe DNA or hybridized electrodes were first immersed into 100 μM $Co(phen)_3^{3+}$ in 0.01 M PBS (pH 7.3) for 20 min, and then the cyclic voltammograms and differential pulse voltammograms were recorded in blank PBS solution.

3. Results and discussions

3.1. Characterization of hollow gold nanospheres (HGN)

In current work, the Co nanoparticles were synthesized with the reduction of Co^{2+} by $NaBH_4$. After the formation of Co nanoparticles, the solution was kept for several minutes to allow excessive $NaBH_4$ to react with water completely (Liang et al., 2004). Because the reduction potential of the $AuCl_4^-$/Au redox couple (0.935 V vs SHE) is much higher than that of the Co^{2+}/Co redox couple (−0.377 V vs SHE), the galvanic replacement reaction as presented in Eq. (1) will occur spontaneously as soon as $AuCl_4^-$ contacts with Co nanoparticles. Fig. 2 shows typical TEM images of samples A–E, where there is a strong contrast difference in all of the spheres with a bright center surrounded by a much darker edge, confirming their hollow architecture. The calculation of the maximum quantities of employed Co nanoparticles and $HAuCl_4$ in the preparation of sample B (See the AppendixBSupplementary Information) indicated that the amount of $HAuCl_4$ in sample B could be just sufficient to react with the added Co nanoparticles completely according to Eq. (1), while the ratio of $HAuCl_4$ in sample A and samples C–E is lower and higher than that in sample B, respectively.

$$3Co + 2AuCl_4^- = 2Au + 3Co^{2+} + 8Cl^- \quad (1)$$

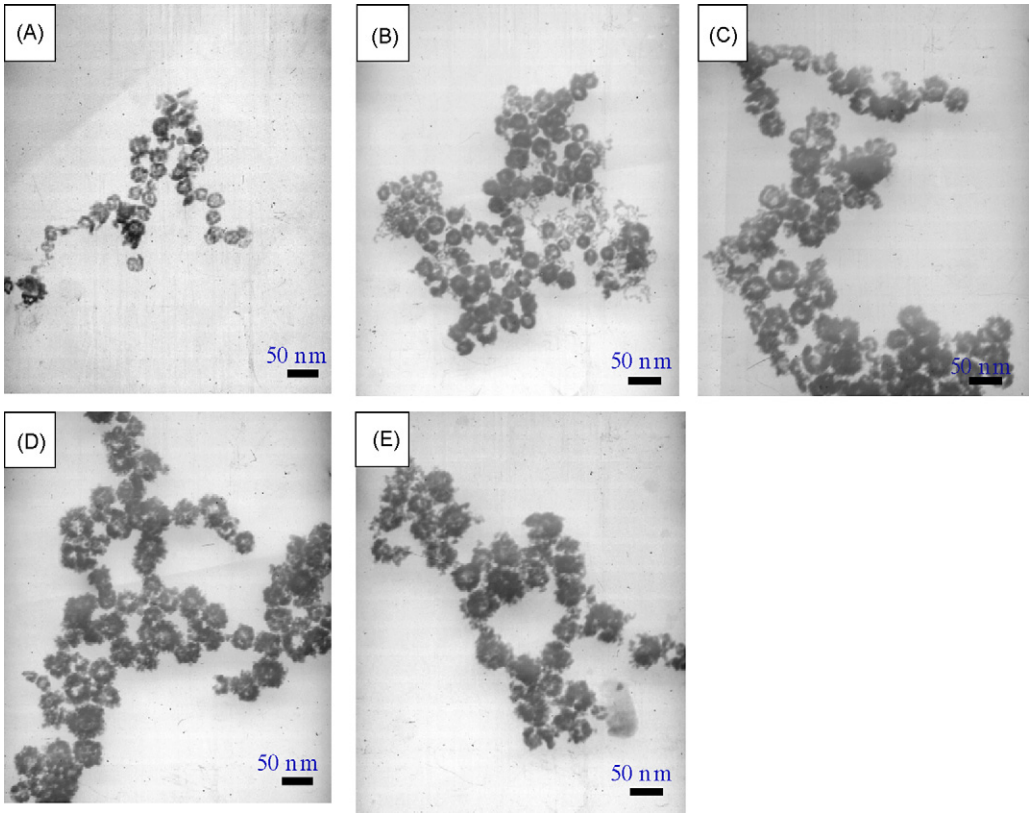

Fig. 2. TEM images of prepared hollow gold nanospheres. Samples of A–E were obtained with the addition of different volumes of 1 mM $HAuCl_4$ into 30 mL Co nanoparticles solution. (A: 5 mL; B: 8 mL; C: 12 mL; D: 18 mL; E: 40 mL).

The hollow gold nanospheres with different shell thickness in sample A (Fig. 2A) was observed, which could be attributed to the fact that some Co nanoparticles react with sufficient $HAuCl_4$ to form a thick shell, while other particles cannot due to the insufficient supply of $HAuCl_4$, thus forming a thin shell. It could be seen from Fig. 2B that the shell of HGN in the sample B became thicker than that of sample A. From the TEM images of samples C–E in Fig. 2, the gold hollow nanospheres are similar to that of sample B except for additional gold nanocrystallite directly connected to the outer shell of gold hollow nanospheres. The existence of citrate molecules was considered to contribute the formation of nanocrystallites around the shell surface. During the fabrication process of HGN, the reduction reaction of $HAuCl_4$ by citrate was considered as a relatively slow process compared with the displacement reaction of Co nanoparticles by $HAuCl_4$. Also, once the Co nanoparticles were completely consumed, the HGN would change from a porous shell surface to a dense surface structure (Liang et al., 2005; Guo et al., 2007). Thus, the free diffusion of $HAuCl_4$ and citrate molecules into the cavity of HGN would be largely inhibited. The excess $HAuCl_4$ molecules in samples C–E would be only reduced at the surface of HGN by citrate molecules. The $HAuCl_4$ has been proved to be reduced by citrate in boiling solution conditions (Frens, 1973). The current reduction of $HAuCl_4$ by citrate at room temperature could be explained according to the mechanism that the HGN was used as the crystal seed and accelerated the autocatalytic growth of gold nanocrystallites at the surface of HGN. With the employed different volumes of $HAuCl_4$ in samples C–E, the different surface morphology around the HGN could be achieved. The samples A and B were observed to have a comparably smooth outer surface and the samples C–E owned the rough surface surrounded with the spike-like nanocrystallites. This structure of spike-like nanocrystallites was especially obvious in sample D (Fig. 2D). With the further increase of $HAuCl_4$ concentration (sample E), the spike-like nanocrystallites tend to aggregate and a sponge-like hollow gold nanosphere starts to form (Fig. 2E). The current prepared hollow gold nanospheres, especially these ones with the outer shell surrounded by spike-like nanocrystallites, should be very favorable for the application in DNA biosensor fabrication due to its large surface area.

3.2. Electrochemical behaviors of $[Fe(CN)_6^{3-/4-}]$ at the modified electrode surface

Fig. 3 shows the cyclic voltammograms obtained for differently modified electrodes in 1 mM $Fe(CN)_6^{3-}/Fe(CN)_6^{4-}$ of 0.1 M KCl at the scan rate of 100 mV s^{-1}. There was a pair of well-defined redox peaks observed on the bare gold electrode with the anodic (E_{pa}) and cathodic (E_{pc}) peak potential of 0.26 and 0.17 V, respectively, and a peak to peak potential separation of about 90 mV (Curve a). These peaks could be definitely attributed to the redox behaviors of $[Fe(CN)_6^{3-/4-}]$. The self-assembly monolayer of 1,6-hexanedithiol on electrode surface largely inhibited the peak current of $[Fe(CN)_6^{3-/4-}]$. This could be easily understood that a relatively compact monolayer of 1,6-hexanedithiol formed on the electrode surface prevents the diffusion of $[Fe(CN)_6^{3-/4-}]$ toward the electrode surface (Curve b). The next modification of HGN on the electrode surface induced a further decrease of peak current (Curve c). The HGN was negative-charged due to the adsorption of citric acid stabilizer and could prevent the diffusion of $[Fe(CN)_6^{3-/4-}]$ toward the electrode surface for the decrease of peak current. It could be observed that the redox peaks of $[Fe(CN)_6^{3-/4-}]$ disappeared in the studied potential range after probe DNA immobilization (Curve d), indicating that the probe DNA has been successfully immobilized on the electrode surface and the diffusion of $[Fe(CN)_6^{3-/4-}]$ toward electrode surface was largely repelled by the negative charged phosphate backbone of probe DNA. The charging current in the studied potential range was

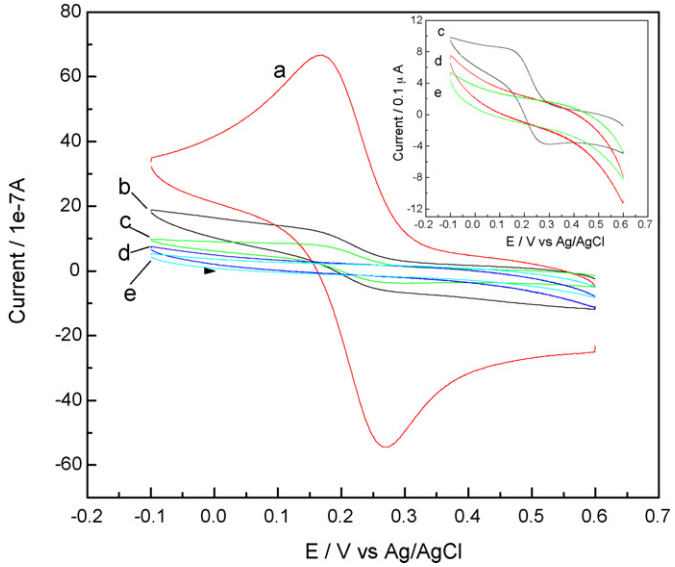

Fig. 3. Cyclic voltammograms obtained for bare (a), 1,6-hexanedithiol modified (b), HGN modified (c), thiolated ssDNA immobilized (d) and hybridized with complementary target DNA modified (e) gold electrodes at 100 mV s^{-1} in $Fe(CN)_6^{3-}/Fe(CN)_6^{4-}$ containing 0.10 M KCl. The concentration of complementary target DNA were 0.01 μM in PBS (0.01 M, pH 7.3). Inset shows the enlarged plot for the curves c–e.

further decreased after hybridization of probe DNA modified electrode with target complementary DNA. This could be well assigned that the introduction of complementary DNA increases the negative charge responsible for the increased repellence of redox species.

Fig. 4 shows the Nyquist plot of the differently modified electrodes in 1 mM $Fe(CN)_6^{3-}/Fe(CN)_6^{4-}$ of 0.1 M KCl at open circuit potential with the frequency varied from 0.01 Hz to 10 kHz. An almost straight line was observed for the bare Au electrode, which was the typical characteristic of a mass diffusion controlled electron transfer process. The Ret was increased to be about 2.4×10^6 Ω with the self-assembly of 1,6-hexanedithiol on the electrode surface. The compact monolayer of 1,6-hexanedithiol on the electrode surface was considered to inhibit the diffusion of $[Fe(CN)_6^{3-/4-}]$

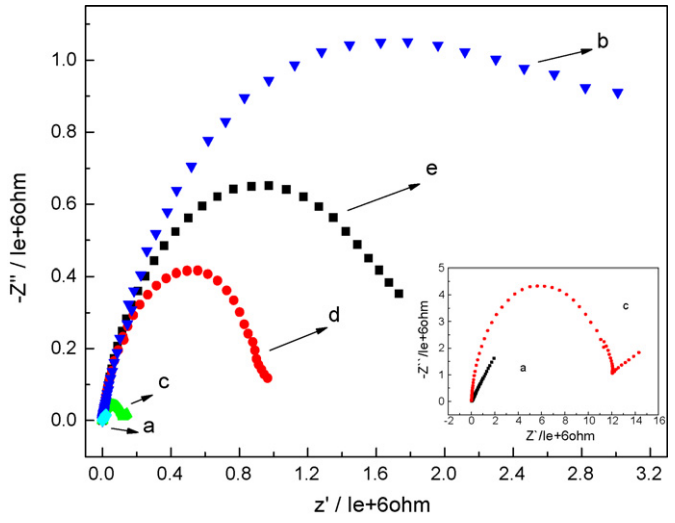

Fig. 4. The Nyquist plots obtained for bare (a), 1,6-hexanedithiol modified (b), HGN modified (c), thiolated ssDNA immobilized (d) and hybridized with complementary target DNA modified (e) gold electrodes in 1 mM $Fe(CN)_6^{3-}/Fe(CN)_6^{4-}$ of 0.1 M KCl at open circuit potential with the frequency varied from 0.01 Hz to 10 kHz. The concentration of complementary target DNA were 0.01 μM in PBS (0.01 M, pH 7.3). Inset shows the enlarged plot for the curve a and c.

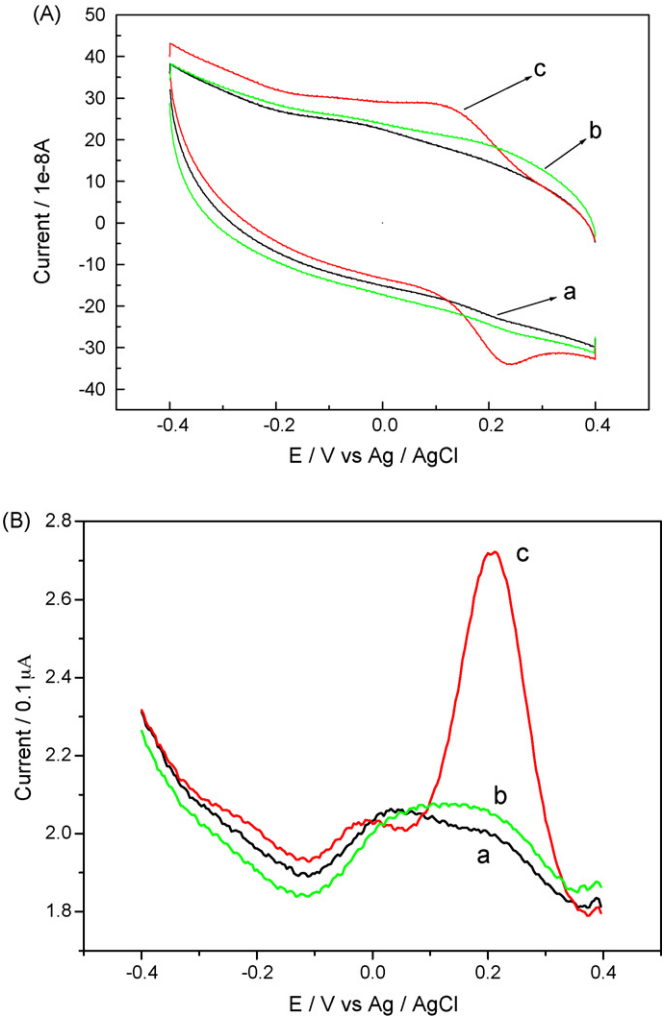

Fig. 5. Cyclic voltammograms (A) and differential pulse voltammograms (B) of ssDNA immobilized (a), hybrids with target DNA (c) and non-complementary target DNA sequence (b) modified electrodes in blank PBS buffer solution after immersion in $Co(phen)_3^{3+}$ for 20 min. The concentration of complementary and non-complementary target DNA were both 0.01 μM in PBS (0.01 M, pH 7.3). The scan rates were all 100 mV s^{-1}.

toward electrode surface and furthermore its electron transfer ability. The Ret value was largely decreased to be about 1.2×10^5 Ω after HGN modification, indicating that the electron transfer ability of $[Fe(CN)_6^{3-/4-}]$ was largely improved by the modified HGN. The Ret values were obtained as about 0.9×10^6 and 1.7×10^6 Ω for the DNA immobilized and hybridized electrodes, respectively. The Ret increase after probe DNA immobilization and hybridization could be well ascribed to the repellence of redox probe from approaching electrode surface by negative charged phosphate skeletons of DNA. The impedance experiments could be well corroborated together with cyclic voltammetry experiments for the characterization of electrode fabrication process.

3.3. *The selectivity of electrochemical DNA biosensor*

Fig. 5A shows the cyclic voltammograms of the differently modified electrode in blank PBS buffer solution after immersion in 0.1 mM $Co(phen)_3^{3+}$ of 0.01 M PBS (pH 7.3) for 20 min. It could be seen that probe DNA immobilization on electrode surface induced no peaks of $Co(phen)_3^{3+}$, indicating that almost no $Co(phen)_3^{3+}$ was adsorbed on the ssDNA chain by the electrostatic interaction mode (Curve a). After hybridization with target DNA, a pair of well-

defined peaks was observed with the anodic and cathodic potential of 0.24 V and 0.12 V, respectively (Curve c). This could be definitely attributed to the redox reaction of $Co(phen)_3^{3+}$ adsorbed into the hybridized duplex DNA by an intercalation mode. The control experiments performed with the hybridization of probe DNA with non-complementary target DNA demonstrated almost the same response with that of only ssDNA modified electrode (Curve b), indicating that $Co(phen)_3^{3+}$ could be used as a good indicator to selectively detect the target DNA.

The DPV experiments using $Co(phen)_3^{3+}$ as an electrochemical hybridization label for detection of different DNA sequences were further advised and the results were shown in Fig. 5B. Only a very small DPV peak current for $Co(phen)_3^{3+}$ was observed at the potential of 0.21 V for the ssDNA immobilized electrode. This indicated that $Co(phen)_3^{3+}$ has a very weak affinity for probe DNA by electrostatic interaction on the modified electrode surface (Curve a). A significant increase of about 0.72×10^{-7} A in the DPV signal was observed after hybridization with fully complementary target DNA (Curve c). When the non-complementary target DNA was used for a control experiment, almost the same peak current with the solely probe DNA immobilized electrode was obtained (Curve b). The selective determination of current fabricated DNA biosensor toward mismatched target DNA was also studied (See Figure S2 in the Supplementary Information). The DPV experiments showed a high selectivity of the constructed DNA biosensor for hybridization detection and the $Co(phen)_3^{3+}$ could be used as a good electrochemical indicator to properly discriminate the ssDNA and dsDNA by our fabricated strategy, which were in good accordance with that of cyclic voltammetry experiments.

The DPV peak current increase before and after hybridization of probe DNA with complementary target DNA was further used to evaluate the performance of current DNA biosensor fabricated on the bare gold electrode and five kinds of HGN (from samples A to E) modified electrodes. The target DNA concentration used was 1×10^{-8} M. The DPV peak current increase for the bare gold and modified electrodes with samples A-E were $0.34 \pm 0.02 \times 10^{-7}$ A, $0.51 \pm 0.02 \times 10^{-7}$ A, $0.59 \pm 0.03 \times 10^{-7}$ A, $0.66 \pm 0.04 \times 10^{-7}$ A, $0.72 \pm 0.03 \times 10^{-7}$ A, $0.68 \pm 0.04 \times 10^{-7}$ A, respectively. Each result was obtained based on three repetitive experiments. The repetitive experiments were performed with three separate bare or HGN modified electrodes. Three gold electrodes were pretreated and simultaneously conducted for dithiol monolayer assembly, HGN modification, DNA immobilization and hybridization, and electrochemical detection according to the same procedures. Thus, a best recognition signal for target DNA could be achieved on the HGN modified electrode with sample D owing to the increased amount of immobilized probe DNA, which was about twice than that of bare gold electrode. This could be explained that the spike-like nanocrystallites around HGN in sample D have an increased surface area for more DNA immobilization and appropriate distribution of nanocrystallites on the HGN surface for optimized hybridization efficiency.

3.4. The sensitivity of fabricated DNA biosensor

It could be seen from Fig. 6A that the peak current change of $Co(phen)_3^{3+}$ on the HGN modified electrode (sample D) increases with the increasing target DNA concentration ranged from 1 pM to 10 nM. In Fig. 6B, the peak current change of fabricated sensor exhibited a linear correlation to the logarithm of the target DNA concentration ranged from 1 pM to 10 nM with a linear regression coefficient of 0.998. The low detection limit was obtained as 1 pM (S/N = 3), which was much better than or comparable to that of other nanomaterials modified electrodes (see Table S1 in the Supplementary Information).

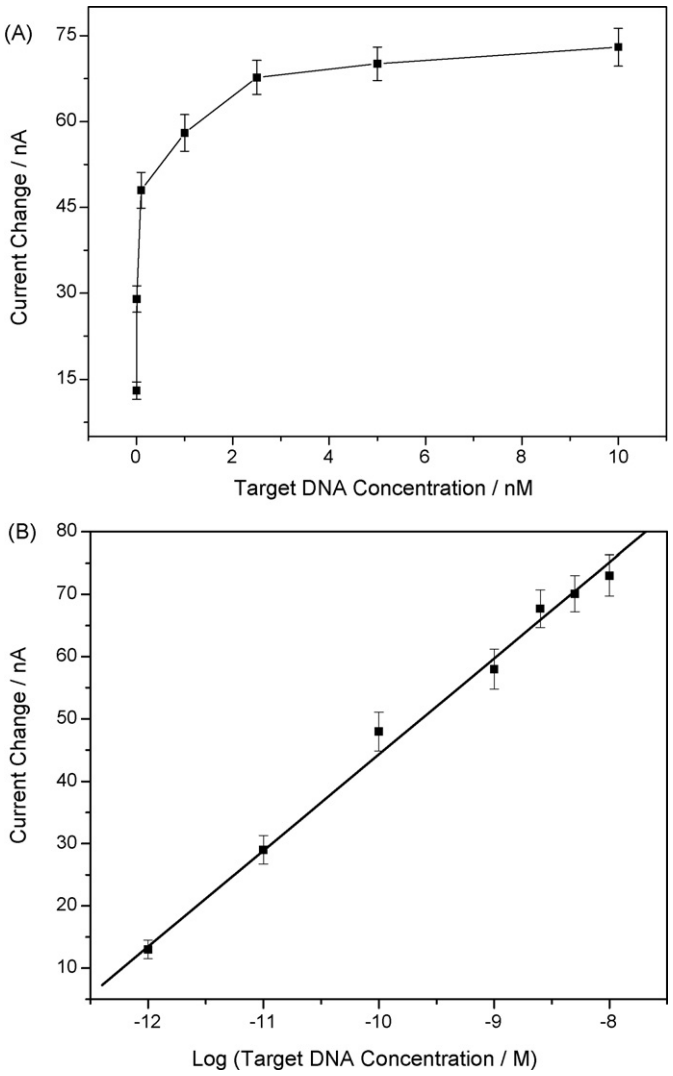

Fig. 6. (A) The plots of DPV peak current change vs the target DNA concentrations. Error bars are the standard deviation of three repetitive experiments. (B) Linear relationship between the DPV peak current change and the logarithm of the target DNA concentration.

3.5. Regeneration and stability of the fabricated DNA biosensor

Regeneration is useful for continuous monitoring of the target DNA in future research. It was found that the fabricated DNA biosensor could be regenerated eight times with about 20% loss of the original signal by dipping the electrode in hot water (80 °C) for 10 min, followed by a rapid cooling in an ice bath for 10 min. The signal attenuation seemed to be attributed to the loss of immobilized HGN and thiolated probes on the electrode surface. At the same time, the stability of the fabricated DNA biosensor was investigated. The probe DNA modified electrode was first stored in the refrigerator at 4 °C over 2 weeks and then examined via DPV after its hybridization with complementary target DNA. Experiments demonstrated that the DNA biosensor retained about 95% of its initial response.

4. Conclusions

An electrochemical DNA biosensor based on the HGN modified electrode was constructed for the enhanced detection of a short DNA sequence. The prepared HGN shows a spike-like morphology of the outer surface, which could upgrade the DNA immobiliza-

tion and hybridization ability. With the use of $Co(phen)_3^{3+}$ as an indicator, the optimized DNA biosensor could achieve a wide linear range from 1 pM to 10 nM for the target DNA detection and a low detection limit of 1 pM. The current fabricated DNA biosensor architecture should be also suitable for the detection of target DNA in real samples, for example clinical analytes. Moreover, this electrode modification strategy was expected for further extensive applications in protein, enzyme biosensors.

Acknowledgement

We thank the Natural Science Foundation of Shandong (grant number Q2008B05, 2009ZRB019J0), the National Natural Science Foundation of China (no. 20775039, 20775038) for their financial supports.

Appendix A. Supplementary data

Supplementary data associated with this article can be found, in the online version, at doi:10.1016/j.bios.2009.11.026.

References

Basuray, S., Senapati, S., Aijian, A., Mahon, A.R., Chang, H., 2009. ACS Nano 3, 1823–1830.
Cai, H, Xu, C., He, P., Fang, Y.Z., 2001. J. Electroanal. Chem. 510, 78–85.
Cederquist, K.B., Golightly, R.S., Keating, C.D., 2008. Langmuir 24, 9162–9171.
Du, P., Li, H., Mei, Z., Liu, S., 2009. Bioelectrochemistry 75, 37–43.
Duan, X., Li, Z., He, F., Wang, S., 2007. J. Am. Chem. Soc. 129, 4154–4155.
Drummond, T.G., Hill, M.G., Barton, J.K., 2003. Nat. Biotechnol. 21, 1192–1199.
Frens, G., 1973. Nature 241, 20–22.
Gasparac, R., Taft, B.J., Lapierre-Devlin, M.A., Lazareck, A.D., Xu, J.M., Kelley, S.O., 2004. J. Am. Chem. Soc. 126, 12270–12271.
Gillard, R.D., Lancashire, R.J., Williams, P.A., 1983. Transition Met. Chem. 8, 188–189.
Gorodetsky, A.A., Buzzeo, M.C., Barton, J.K., 2008. Bioconjugate Chem. 19, 2285–2296.
Gunnarsson, A., Jönsson, P., Marie, R., Tegenfeldt, J.O., Höök, F., 2008. Nano Lett. 8, 183–188.
Guo, S., Fang, Y., Dong, S., Wang, E., 2007. J. Phys. Chem. C 111, 17104–17109.
Hu, K., Lan, D., Li, X., Zhang, S., 2008. Anal. Chem. 80, 9124–9130.
Jena, B.K., Raj, C.R., 2007. J. Phys. Chem. C 111, 6228–6232.
Kara, P., Kerman, K., Ozkan, D., Meric, B., Erdem, A., Ozkan, Z., Ozsoz, M., 2002. Electrochem. Commun. 4, 705–709.
Kim, D., Kerman, K., Saito, M., Sathuluri, R.R., Endo, T., Yamamura, S., Kwon, Y., Tamiya, E., 2007. Anal. Chem. 79, 1855–1864.
Kim, S., Kim, M., Lee, W.Y., Hyeon, T., 2002. J. Am. Chem. Soc. 124, 7642–7643.
Kjällman, T.H.M., Peng, H., Soeller, C., Travas-Sejdic, J., 2008. Anal. Chem. 80, 9460–9466.
Kobayashi, Y., Horie, M., Konno, M., Rodríguez-González, B., Liz-Marzán, L.M., 2003. J. Phys. Chem. B 107, 7420–7425.
Li, D., Yan, Y., Wieckowska, A., Willner, I., 2007. Chem. Commun. 34, 3544–3546.
Liang, H., Wan, L., Bai, C., Jiang, L., 2005. J. Phys. Chem. B 109, 7795–7800.
Liang, H., Zhang, H., Hu, J., Guo, Y., Wan, L., Bai, C., 2004. Angew. Chem. Int. Ed. 43, 1540–1543.
Liu, G., Wan, Y., Gau, V., Zhang, J., Wang, L., Song, S., Fan, C., 2008. J. Am. Chem. Soc. 130, 6820–6825.
Liu, S., Li, Y., Li, J., Jiang, L., 2005. Biosens. Bioelectron. 21, 789–795.
Liu, T., Tang, J.A., Zhao, H.Q., Deng, Y.P., Jiang, L., 2002a. Langmuir 18, 5624–5626.
Liu, T., Tang, J.A., Jiang, L., 2002b. Biochem. Biophys. Res. Commun. 295, 14–16.
Lu, W., Wang, W., Su, Y., Li, J., Jiang, L., 2005. Nanotechnology 16, 2582–2586.
Lu, W., Lin, L., Jiang, L., 2007. Biosens. Bioelectron. 22, 1101–1105.
March, G., Noël, V., Piro, B., Reisberg, S., Pham, M., 2008. J. Am. Chem. Soc. 130, 15752–15753.
Minunni, M., Tombelli, S., Fonti, J., Spiriti, M.M., Mascini, M., Bogani, P., Buiatti, M., 2005. J. Am. Chem. Soc. 127, 7966–7967.
Munde, M., Ismail, M.A., Arafa, R., Peixoto, P., Collar, C.J., Liu, Y., Hu, L., David-Cordonnier, M., Lansiaux, A., Bailly, C., Boykin, D.W., Wilson, W.D., 2007. J. Am. Chem. Soc. 129, 13732–13743.
Patolsky, F., Lichtenstein, A., Willner, I., 2000. J. Am. Chem. Soc. 122, 418–419.
Schmidt, H.T., Ostafin, A.E., 2002. Adv. Mater. 14, 532–535.
Sun, Y., Xia, Y., 2002a. Anal. Chem. 74, 5297–5305.
Sun, Y., Xia, Y., 2002b. Science 298, 2176–2179.
Taton, T.A., Mirkin, C.A., Letsinger, R.L., 2000. Science 289, 1757–1760.
Wong, M.S., Cha, J.N., Choi, K., Deming, T.J., Stucky, G.D., 2002. Nano Lett. 2, 583–587.
Yang, R., Jin, J., Chen, Y., Shao, N., Kang, H., Xiao, Z., Tang, Z., Wu, Y., Zhu, Z., Tan, W., 2008. J. Am. Chem. Soc. 130, 8351–8358.
Yamada, M., Tadera, T., Kubo, K., Nishihara, H., 2003. J. Phys. Chem. B 107, 3703–3711.
Zhang, G., Zhang, G., Chua, J.H., Chee, R., Wong, E.H., Agarwal, A., Buddharaju, K.D., Singh, N., Gao, Z., Balasubramanian, N., 2008a. Nano Lett. 8, 1066–1070.
Zhang, J., Qi, H., Li, Y., Yang, J., Gao, Q., Zhang, C., 2008b. Anal. Chem. 80, 2888–2894.
Zhang, X., Jiao, K., Liu, S., Hu, Y., 2009a. Anal. Chem. 81, 6006–6012.
Zhang, Y., Wang, Y., Wang, H., Jiang, J., Shen, G., Yu, R., Li, J., 2009b. Anal. Chem. 81, 1982–1987.
Zhao, L., Siu, A.C.L., Petrus, J.A., He, Z., Leung, K.T., 2007. J. Am. Chem. Soc. 129, 5730–5734.
Zhu, D., Tang, Y., Xing, D., Chen, W.R., 2008. Anal. Chem. 80 (10), 3566–3571.